Triple-Resonance Multidimensional NMR Study of Calmodulin Complexed with the Binding Domain of Skeletal Muscle Myosin Light-Chain Kinase: Indication of a Conformational Change in the Central Helix[†]

Mitsuhiko Ikura,[‡] Lewis E. Kay,[‡] Marie Krinks,[§] and Ad Bax*,[‡]

Laboratory of Chemical Physics, National Institute of Diabetes and Digestive and Kidney Diseases, and Laboratory of Biochemistry, National Cancer Institute, National Institutes of Health, Bethesda, Maryland 20892

Received November 27, 1990; Revised Manuscript Received January 28, 1991

ABSTRACT: Heteronuclear 3D and 4D NMR experiments have been used to obtain ^1H, ^{13}C, and ^{15}N backbone chemical shift assignments in Ca^{2+}-loaded calmodulin complexed with a 26-residue synthetic peptide (M13) corresponding to the calmodulin-binding domain (residues 577–602) of rabbit skeletal muscle myosin light-chain kinase. Comparison of the chemical shift values with those observed in peptide-free calmodulin [Ikura, M., Kay, L. E., & Bax, A. (1990) *Biochemistry 29*, 4659–4667] shows that binding of M13 peptide induces substantial chemical shift changes that are not localized in one particular region of the protein. The largest changes are found in the first helix of the Ca^{2+}-binding site I (E11–E14), the N-terminal portion of the central helix (M72–D78), and the second helix of the Ca^{2+}-binding site IV (F141–M145). Analysis of backbone NOE connectivities indicates a change from α-helical to an extended conformation for residues 75–77 upon complexation with M13. This conformational change is supported by upfield changes in the $C\alpha$ and carbonyl chemical shifts of these residues relative to M13-free calmodulin and by hydrogen-exchange experiments that indicate that the amide protons of residues 75–82 are in fast exchange ($k_{exch} > 10 \text{ s}^{-1}$ at pH 7, 35 °C) with the solvent. No changes in secondary structure are observed for the first helix of site I or the C-terminal helix of site IV. Upon complexation with M13, a significant decrease in the amide exchange rate is observed for residues T110, L112, G113, and E114 at the end of the second helix of site III.

The molecular recognition of intracellular enzymes and regulatory proteins by calmodulin (CaM)[1] plays a key role in coupling Ca^{2+} transients caused by a stimulus at the cell surface to events in the cytosol. The crystal structure of CaM shows an unusual dumbbell shape consisting of a long central helix and two globular homologous domains each containing two helix–loop–helix calcium-binding motifs of the so-called "EF-hand" type (Babu et al., 1988; Kretsinger et al., 1986). Both domains have a hydrophobic patch that is considered capable of binding to several hydrophobic drugs that inhibit CaM activity. These patches presumably also form the binding site for the target protein. Binding studies with small naturally occurring biologically active peptides and synthetic analogues clearly indicate that CaM has a high affinity for positively charged amphiphilic α-helices (Anderson & Malencik, 1986; O'Neil & Degrado, 1990). The propensity to form an amphiphilic helix was also reported for the CaM-binding domains of several CaM-dependent enzymes, for which the amino acid sequence has been determined [for a review, see Blumenthal and Krebs (1988)].

The interaction between CaM and its target enzymes has been studied by a variety of chemical and physicochemical methods [see Klee (1988) for a review]. Small-angle X-ray scattering studies on the CaM complexes with mastoparan (Matsushima et al., 1989), with melittin (Kataoka et al., 1989), and with a 26 amino acid CaM-binding fragment of skeletal muscle myosin light-chain kinase (MLCK) known as M13 (Heidorn et al., 1989) indicated that the two globular domains

in those complexes are much closer together than in the crystal structure of uncomplexed calmodulin, suggesting a disruption of the central-helix feature observed in the crystal structure. Jackson et al. (1986) showed that three of the lysine residues (K21, K75, and K148) are significantly protected from acetylation when CaM is complexed with MLCK. Manalan and Klee (1987) reported that calcineurin also protects K75 and K148 from acetylation. ^1H and ^{113}Cd NMR studies showed that when calmodulin binds target peptides, substantial chemical shift changes occur in the spectra of both domains (Klevit et al., 1985; Seeholzer et al., 1986; Linse et al., 1986; Ikura et al., 1989). However, no direct evidence has been obtained regarding the exact location where changes in the structure of calmodulin take place upon binding of target peptide. The most detailed NMR analysis of the complex of CaM with a MLCK fragment (Seeholzer & Wand, 1989) showed that despite substantial chemical shift changes in the two short antiparallel β-sheet regions of the two globular domains, the secondary structure of these regions was preserved.

Using novel heteronuclear triple-resonance (^1H,^{13}C,^{15}N) three-dimensional NMR techniques (Kay et al., 1990b), we recently were able to make complete backbone ^1H, ^{13}C, and ^{15}N assignments of CaM ($M_r \sim 16.7$ kDa). This protein was

---

[1] Abbreviation: CaM, Calmodulin; HCACO, α-proton to α-carbon to carbonyl correlation; HCACON, α-proton to α-carbon to carbonyl to nitrogen correlation; HCA(CO)N, α-proton to α-carbon (via carbonyl) to nitrogen correlation; H(CA)NH, α-proton (via α-carbon) to nitrogen to amide proton correlation; HMQC, heteronuclear multiple-quantum correlation; HNCO, amide proton to nitrogen to carbonyl correlation; HOHAHA, homonuclear Hartmann–Hahn; MLCK, myosin light-chain kinase; M13, a 26-residue fragment of the CaM-binding domain of MLCK comprising residues 577–602; NMR, nuclear magnetic resonance; TPPI, time-proportional phase incrementation; 2D, two dimensional; 3D, three dimensional; 4D, four dimensional.

the first example for which backbone assignments were obtained with this approach (Ikura et al., 1990a). Here we report results of this new approach for studying the CaM–M13 complex. The larger molecular weight of the CaM–M13 complex (19.7 kDa) and the concomittant increase in line width forced us to use a slightly modified procedure from that described previously. In this new procedure the only experimental step that relied on poorly resolved ^1H–^1H J coupling, the HOHAHA–HMQC experiment (Marion et al., 1989b), is replaced by a triple-resonance technique that relies entirely on single-bond heteronuclear couplings for correlating HN and Hα chemical shifts (Kay et al., 1991a). In addition, a four-dimensional (4D) NMR experiment is used to facilitate automated assignment for spectra of the complexity as that obtained for CaM–M13. The present paper briefly describes the improved triple-resonance approach and reports the ^1H, ^{13}C, and ^{15}N CaM backbone assignments for the CaM–M13 complex. A chemical shift comparison is made with values found for M13-free Ca^{2+}-ligated CaM. In addition, NOEs are reported for amide protons in the central helix part of CaM where substantial chemical shift changes occur, and these NOEs are compared with patterns observed for uncomplexed CaM.

EXPERIMENTAL PROCEDURES

Sample Preparation. *Drosophila* CaM was over expressed by using the pAS vector in *Escherichia coli* (strain AR58) and was purified as reported previously (Ikura et al., 1990a,b). Samples used for the NOE and hydrogen-exchange experiments contained uniformly ^{15}N-labeled (~95%) CaM in H_2O solution; all other experiments were carried out on ^{15}N- and ^{13}C-labeled (~95%) CaM, in either H_2O or D_2O solution. Chemically synthesized HPLC-purified peptide M13 (KRRWKKNFIAVSAANRFKKISSSGAL) (Peptide Technologies Corp. Washington, D.C.) was used without further purification. NMR samples were prepared according to the procedure outlined by Seeholzer and Wand (1989): 12 mg of decalcified CaM was dissolved in 4.5 mL of H_2O solution containing 0.01 M KCl and 0.68 mM $CaCl_2$, and the pH was adjusted to 6.8. The concentration of CaM (0.16 mM) in this solution was determined by UV spectroscopy with an extinction coefficient ($\epsilon^{1\%}_{276nm}$) of 0.945 in the presence of Ca^{2+}. M13 stock solution (0.18 mM) was added slowly to the CaM solution until the concentration ratio of M13 and CaM reached 1:1. No precipitation was observed under these conditions. The solution was concentrated without freezing by using a speed vacuum concentrator to a total volume of 0.43 mL after which 0.02 mL of D_2O was added for a deuterium lock, and the pH was readjusted to 6.8. In the final NMR sample, the concentration of the complex was 1.5 mM. The D_2O sample was prepared as described above, except that D_2O was used as solvent, with 7 mg of calmodulin, resulting in a final sample concentration of 1.0 mM.

NMR Spectroscopy. With the exception of the ^{15}N 3D NOESY-HMQC experiment, all NMR experiments were carried out at 36 °C on a Bruker AM-500 spectrometer, equipped with a triple-resonance probe head optimized for ^1H detection, and home-built hardware (Kay et al., 1990b) to minimize overhead time and to generate the frequencies for the third channel. The pulse sequences used for the triple-resonance 3D and 4D experiments have been described previously (Ikura et al., 1990a; Kay et al., 1990b, 1991a,b).

The HNCO and HNCA 3D spectra, recorded in H_2O, result from matrices comprising 32 complex × 64 complex × 1024 real data points. The spectral widths used in F_1 and F_3 were 1000 and 8064 Hz, respectively, with corresponding

acquisition times of 32.0 and 63.5 ms. The F_3 carrier was set at the water resonance position to ensure that zero-frequency artifacts fall outside the spectral region of interest. For HNCO, the F_2 (C′) spectral width was 1388.9 Hz (acquisition time 46.1 ms). For HNCA, the F_2 (Cα) spectral width was 4310 Hz (acquisition time 14.8 ms). For the HCACO and HCA(CO)N 3D experiments, recorded in D_2O solution, the acquired data matrices comprised 32 complex × 64 complex × 512 real data points. The spectral widths in F_1 (Cα) and F_3 (Hα) were 2994 and 5000 Hz, respectively, with corresponding acquisition times of 10.7 and 51.2 ms. For the HCACO experiment, the F_2 (C′) spectral width was 1389 Hz (acquisition time 46.1 ms) and 1000 Hz (acquisition time 32 ms) for the F_2 (^{15}N) dimension of the HCA(CO)N experiment. The H(CA)NHN spectrum, recorded in H_2O, resulted from a 64 complex × 32 complex × 1024 real data matrix with spectral widths of 2180 Hz (F_1, Hα), 1000 Hz (F_2, ^{15}N), and 8250 Hz (F_3, HN), and acquisition times of 29.4, 32, and 62 ms, respectively. The total measuring time needed for recording all four 3D triple-resonance experiments was about 9 days. In the t_1 and t_2 dimensions of all 3D experiments, complex data were acquired in a States-TPPI manner (Marion et al., 1989a). For the HNCO, HNCA, and H(CA)NHN, the length of the ^{15}N time domain data was extended to 64 complex points by using linear prediction. For HCACO, the t_2 domain (C′) was extended to 128 complex points in the same manner. In addition, zero filling was employed in all dimensions prior to Fourier transformation. For the HNCO, HNCA, and H(CA)NHN experiments, the right half of the spectrum in the F_3 dimension (upfield of H_2O), where there is no signal, was discarded after F_3 Fourier transformation. The absorptive part of the final processed data matrix comprised 256 × 128 × 512 points for all 3D spectra.

The HCACON 4D spectrum was recorded as described previously (Kay et al., 1991b). The size of the acquired data matrix was 32 complex × 8 complex × 8 complex × 512 real. The t_2 and t_3 data were extended to 16 complex points by using linear prediction. Zero filling was used in all dimensions. The spectral widths were 2994, 1388.9, 1000, and 5000 Hz in the F_1, F_2, F_3, and F_4 dimensions, respectively.

Spin system identification was made for a substantial number of amino acids with the HCCH-COSY technique (Kay et al., 1990a), which correlates vicinal protons via a three-step $^1H \rightarrow {}^{13}C$, $^{13}C \rightarrow {}^{13}C$, $^{13}C \rightarrow {}^1H$ magnetization transfer. The spectrum, recorded in D_2O, resulted from a 64 complex × 32 complex × 512 real data matrix, with acquisition times of 25.6 ms (F_1, ^1H), 10.7 ms (F_2, ^{13}C), and 51.2 ms (F_3, ^1H). Linear prediction was used in the F_1 dimension to double the length of the time domain data, and zero filling was used in all dimensions.

A 3D ^{15}N-separated 3D NOESY-HMQC experiment was carried out at 36 °C on a Bruker AM-600 spectrometer, with a pulse sequence that does not require presaturation of the H_2O resonance (Messerle et al., 1989). The size of the acquired data matrix was 128 complex × 16 complex × 512 real, with acquisition times of 21.3 ms (F_1, ^1H), 13.3 ms (F_2, ^{15}N), and 56.3 ms (F_3, ^1H). The t_2 time domain was extended to twice its original length by using linear prediction, and zero filling was used in all three dimensions prior to Fourier transformation.

The 3D and 4D data were processed on a Sun Sparc-1 workstation and on a Sun-4 using simple in-house routines for Fourier transformation in the F_2 dimension (Kay et al., 1989) and linear prediction together with the commercially available software package NMR2 (New Methods Research, Inc., Syr-
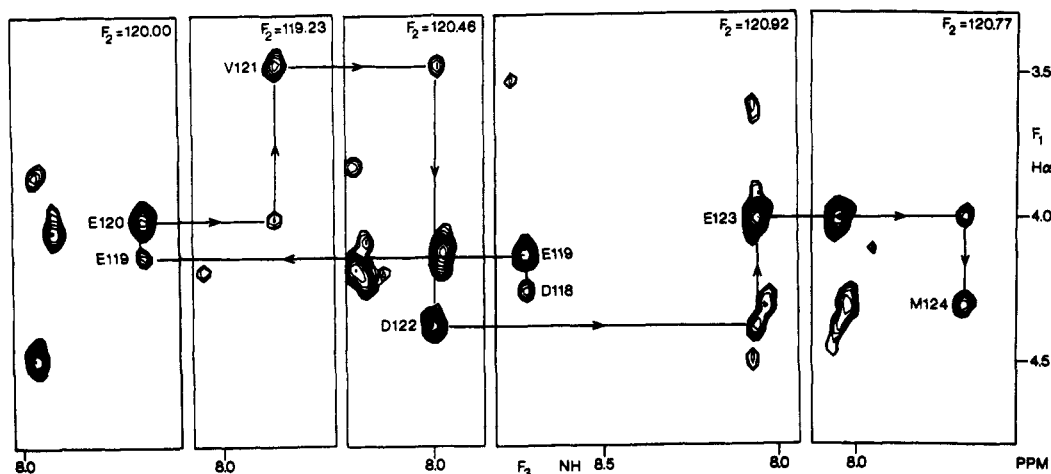
FIGURE 1: Selected F_1/F_3 cross sections of the H(CA)NHN 3D spectrum of the CaM–M13 complex, illustrating sequential connectivity for residues D118 through M124.

acuse, NY) for processing the F_1–F_3 planes in 3D spectra and F_1–F_4 planes of the 4D spectrum.

Amide hydrogen-exchange rates for rapidly exchanging amide resonances were measured by using a jump-and-return heteronuclear multiple-quantum correlation experiment (Roy et al, 1984) with and without presaturation of the water resonance. To distinguish amide exchange effects from amide attenuation occuring via spin diffusion, the experiment was performed both at pH 6.8 and 6.3. Only in cases where the attenuation of the amide resonance occurring upon presaturation of the H_2O resonance is stronger at the higher pH is this interpreted as positive evidence for amide exchange. Details of this procedure are presented elsewhere (Spera et al., 1991).

The 0.5 pH unit difference between the free CaM study and the present one does not cause any ^1H chemical shift changes larger than 0.02 ppm or ^{15}N changes larger than 0.1 ppm, with the exception of residues L18, H107, T110, and G113, where small but observable shift changes are noticeable. The 11 °C lower temperature in the present study causes small (<0.1 ppm) differences in the HN shift, which are not accounted for in our comparison of chemical shifts.

RESULTS

As reported by Klevit et al. (1985) and Seeholzer and Wand (1989), in the presence of substoichiometric amounts of peptide, the NMR spectrum is composed of two distinct sets of resonances from free CaM and from the 1:1 CaM–M13 complex. This slow-exchange phenomenon on the NMR time scale is caused by a very small dissociation constant of ~1 nM (Blumenthal et al., 1985). The stoichiometry of CaM and M13 in the sample was verified by the relative intensity of these two sets of resonances in a 2D ^1H–^{15}N shift correlation spectrum (Bodenhausen & Ruben, 1980). The first attempt to make a 1:1 CaM–M13 complex resulted in a substoichiometric (1:0.87) amount of peptide, presumably resulting from the fact that the peptide concentration was lower than expected on the basis of the weight of the dissolved peptide. In the ^1H–^{15}N shift correlation 2D spectrum, at least 90% of the cross peaks are affected to such an extent by the addition of M13 that assignment is not possible by simple comparison of the two ^{15}N–^1H correlation spectra (supplementary material). Therefore, rather than attempting to assign the spectrum of the complex by comparison with the chemical shifts of free CaM, we decided to start the procedure de novo using previously developed triple-resonance methodology (Ikura et al., 1990a) in combination with several new experiments.

Although the total molecular weight of the CaM–M13 complex is increased by ~3 kDa over free CaM, the amount of overlap in the ^1H–^{15}N correlation spectrum actually decreases. However, the rotational correlation time τ_c for the complex in the present study was significantly longer than for free CaM, owing to an 18% increase in the weight of the complex and the 11 °C lower temperature used in the present study. As a result, a substantial number of the α-helical HN–Hα couplings (~4 Hz) were too small to give rise to an observable HN–Hα correlation in the ^{15}N HOHAHA-HMQC 3D spectrum. Therefore, a new 3D technique, named H-(CA)NHN, was developed to obtain this information (Kay et al., 1991a). The H(CA)NHN experiment utilizes only one-bond couplings to relay the magnetization from Hα to HN, and therefore magnetization transfer efficiency is not affected by secondary structure, although the sensitivity of the experiment is uniformly reduced by the relatively large $^{13}C\alpha$ line width and the passive $^{13}C\alpha$–$^{13}C\beta$ J coupling. In addition to intraresidue HN–Hα J connectivity, the H(CA)NHN experiment frequently also provides interresidue connectivity between HN$_i$ and Hα_{i-1} via the two-bond ^{15}N–$^{13}C\alpha$ coupling, analogous to the HNCA experiment, which can provide connectivity between HN$_i$ and Cα_{i-1}. As an example of the power of this new technique, Figure 1 shows selected regions of slices of the 3D H(CA)NHN spectrum, illustrating the sequential connectivity for residues 118–124. The H(CA)NHN experiment does not require presaturation of the H_2O resonance and thus allows observation of HN–^{15}N–Hα connectivities for residues with amide protons that are in rapid exchange with solvent. This feature of the H(CA)NHN experiment was crucial for assigning several of the amide resonances in the central helix that are obliterated by H_2O presaturation.

The spectral assignment procedure used in the present work is improved over the one reported previously (Ikura et al., 1990a) and now consists of the following steps:

(i) Peak coordinate tables for each of HNCO, HNCA, H(CA)NHN, HCACO, and HCA(CO)N 3D spectra and for the HCACON 4D spectrum are obtained in an automated manner. Manual editing of these peak tables is used to delete artifactual peaks and to make adjustments for overlapping resonances. In addition, chemical shifts for resonances that are folded in the ^{15}N dimension are adjusted.

(ii) A set of spin systems is constructed that contain the chemical shifts of the amino acid head: HN$_i$, N$_i$, Cα_i, Hα_i, Hα_{i-1}, Cα_{i-1}, and C$'_{i-1}$. This is accomplished by searching for pairs of peaks with identical N$_i$ and HN$_i$ chemical shifts in the HNCO, HNCA, and H(CA)NHN peak coordinate tables.

At a first stage, the program searches for unique N_i/HN_i pairs using relatively large error margins (0.2 ppm for ^{15}N and 0.02 ppm for HN). For most of the remaining nonunique N_i/HN_i pairs, visual inspection of plotted 3D spectra provides a rapid means to determine the correct sets of corresponding chemical shifts. In the HNCA spectrum, $C\alpha_{i-1}$ and $C\alpha_i$ are distinguished by the fact that the correlation to $C\alpha_{i-1}$ is invariably the weakest of the two. Similarly, in the H(CA)NHN spectrum, the correlation to $H\alpha_{i-1}$ is always weaker than the correlation to $H\alpha_i$. Note that for proline residues and for residues with rapidly exchanging amide protons no correlation is observed in the HNCO and HNCA spectra, causing the absence of the head spin system of these residues. Provided the amide exchange rate is not too fast ($< \sim 50$ s^{-1}) correlations for the rapidly exchanging amides can be observed with the H(CA)NHN experiment, which does not employ presaturation of the H_2O resonance.

(iii) A second set of spin systems is constructed that contains the chemical shifts of the amino acid tail: $C\alpha_i$, $H\alpha_i$, CO_i, and N_{i+1}. This is accomplished by searching for correlations with identical $C\alpha$ and $H\alpha$ chemical shifts in the HCACO and HCA(CO)N spectra. In principle, this step can be eliminated by recording the 4D HCA(CO)N spectrum. In practice, the resolution in the 4D spectrum is limited, and analysis of the 3D spectra provides the most accurate C′ and ^{15}N shift values. However, the 4D spectrum can fruitfully be used to remove ambiguities that occur if two pairs of $H\alpha$ and $C\alpha$ resonances exactly overlap. In this case, it is not possible on the basis of the HCACO and HCA(CO)N spectra alone to decide which of the two C′ resonances is coupled to which of the two ^{15}N resonances, whereas the 4D experiment provides the answer by inspection. This is illustrated for residues D24 and D56 in the supplementary material.

(iv) The next step consolidates the information present in the "head" and the "tail" spin systems mentioned above to generate "amino acid spin systems" by comparing the $H\alpha$ and $C\alpha$ chemical shifts of each of the smaller spin systems. Each amino acid spin system now contains the chemical shift values of HN_i, N_i, $H\alpha_i$, $C\alpha_i$, and CO_i and for most residues also the shift of the adjacent nuclei $C\alpha_{i-1}$, $H\alpha_{i-1}$, CO_{i-1}, and N_{i+1}. A total of 142 CO_{i-1}, 108 $C\alpha_{i-1}$, 66 $H\alpha_{i-1}$, and 135 N_{i+1} connectivities are observed. Because of the relatively small dispersion in both $C\alpha$ and $H\alpha$ chemical shifts, a substantial number of head–tail combinations are not unique and are marked as such. At this stage, information is added regarding the amino acid side chain, by using the 3D HCCH-COSY experiment (Kay et al., 1990a). In fact, all 11 Gly, 10 Ala, 13 Thr, 7 Val, and 5 Ile were identified in the CaM–M13 complex at this stage. Even this limited number of spin system identifications is more than sufficient to complete the backbone assignment process because of the high degree of redundancy in sequential connectivity information. Complete side-chain assignment is obtained most easily by using the combination of HCCH-COSY and HCCH-TOCSY (Fesik et al., 1990; Bax et al. 1990) and will be reported elsewhere.

(v) The next step proceeds to link the spin systems identified in step iv to generate peptide spin systems. This is accomplished by linking the unique amino acid spin systems, comparing the groups of chemical shifts of each of the amino acid spin systems. For each group of unambiguously linked amino acids, it is verified at this stage whether the amino acid types are compatible with the protein amino acid sequence.

(vi) The final step of the backbone assignment uses the information of the "non-unique" amino acid spin systems, mentioned in step iv, combined with the amino acid type in-

formation to provide the correct linkages between the peptide spin systems.

Use of the assignment procedure outlined above led to unambiguous and complete ^1H, ^{13}C, and ^{15}N resonance assignment for the protein backbone in the CaM–M13 complex. The chemical shifts are reported in Table I.

Discussion

The 2D ^1H NMR study of the complex between bovine brain CaM and a 19-residue MLCK peptide (Seeholzer & Wand, 1989) showed substantial chemical shift changes for HN and $H\alpha$ protons for many of the 27 residues for which assignments were obtained. Comparison of these partial assignments with our present results, obtained for engineered CaM complexed with the 26-residue MLCK peptide, shows virtually identical chemical shift changes for these residues. This close agreement suggests that the C-terminal part of M13 (consisting of residues KKISSSGAL) does not significantly affect any of the chemical shifts reported by Seeholzer and Wand. Engineered *Drosophila* CaM used in our present study lacks the ε-trimethyl group at K115 and the N-terminal acetyl group present in natural CaM and contains three amino acid substitutions relative to bovine CaM: Y99 → F99, Q143 → T143, and A147 → S147. Neither these sequence differences nor the absence of the posttranslational modifications in engineered CaM nor the additional N-terminal acetylmethionine of the 19-residue peptide has any observable effect on the HN and $H\alpha$ chemical shifts of the 27 residues for which assignments previously were reported.

The triple-resonance assignment procedure yields considerably more information than ^1H assignments alone, since for each residue chemical shifts of all five backbone nuclei are obtained. The $C\alpha$ and C′ chemical shifts in particular are quite sensitive to secondary structure, and there is a clear correlation that in α-helical structures these nuclei resonate downfield (larger ppm numbers) relative to the same residue in an extended structure such as β-sheet [for a review, see Saito (1986)]. $H\alpha$ chemical shifts show a similar but opposite correlation with secondary structure, albeit weaker (Clayden & Williams, 1982; Szilagyi & Jardetzky, 1989; Pastore & Saudek, 1990). The HN proton chemical shift has been related to the strength of hydrogen bonding (Wagner et al., 1983), with stronger hydrogen bonding resulting in a downfield shift, but the HN chemical shift is also sensitive to a number of other factors. For ^{15}N, amides in β-sheeted regions tend to be shifted downfield from amides in α-helical regions (Shoji et al., 1987), but large ^{15}N shift variations within these regions of secondary structure remain poorly understood (Glushka et al., 1989).

Figure 2 shows the change in chemical shifts observed upon complexation of CaM with M13.[2] The bottom graph in Figure 2 presents a weighted average of the chemical shift changes observed for each residue and gives a rough indication of the extent to which a residue is affected by complexation with M13. Overall appearance indicates that M13 binding affects chemical shifts in the entire protein. However, the most significant changes are localized in three regions of the molecule: the N-terminal portion of the central helix (M72–D78), the E helix of the EF-hand in the Ca^{2+}-binding domain I (E11–E14), and the F helix in the Ca^{2+}-binding domain IV (F141–M145).

---

[2] The ^{15}N chemical shifts of two prolines (P43 and P66) previously reported for free CaM (Ikura et al., 1990a) were not corrected for folding and should be read as 135.3 (P43) and 136.9 ppm (P66). $C\alpha$ chemical shifts of E11 and K77 of free CaM were reported incorrectly and should be 59.5 and 56.7 ppm, respectively.
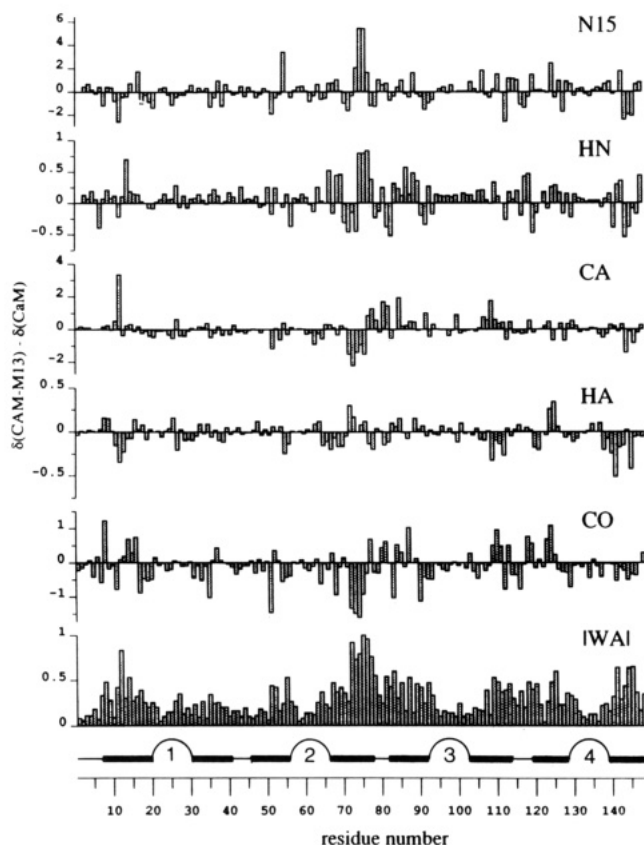
FIGURE 2: Plots of the change in chemical shift for the five backbone atoms, occurring upon complexation of CaM with M13 as a function of residue number. The bottom graph presents a weighted average, $|WA|$, over the changes of all five backbone atoms, using the formula $|WA| = \sum |\delta_{CaM-M13} - \delta_{CaM}| / |\Delta_{max}|$, where the summation extends over the five backbone atoms, $\delta_{CaM-M13}$ and δ_{CaM} are the chemical shifts observed in the complex and in free CaM, and Δ_{max} is the largest chemical shift change observed for each type of nucleus. The position of the four calcium binding domains and of the α-helices observed in the crystal structure are indicated above the horizontal axis.

FIGURE 3: Comparison of the sequential NOE connectivties involving HN and Hα protons of the central helix portion (residues 68–92) in free CaM and in the CaM–M13 complex. The NOE intensities are indicated by the black bars and classified into three levels, strong, medium, and weak. The $d_{\alpha N}$ connectivity between D80 and S81 in CaM–M13 is tentative because it is partly obscured by overlap with the intense H$_2$O resonance.

Comparison of the 3D NOE data for CaM and CaM–M13 (data not shown) suggests that backbone conformations of the E helix of domain I and the F helix of domain IV remain intact upon complexation with M13. Comparing the central helix backbone NOE connectivities observed for free and complexed CaM (Figure 3) suggests that in the complex the α-helical structure of CaM gets disrupted abruptly starting at residue K75. Upfield changes in Cα and C' chemical shifts together with downfield changes in Hα chemical shift observed for residues 72–76 suggest that the distortion of the central helix may start actually as early as residue 72. Hydrogen-exchange experiments indicate rapid amide exchange for residues K75 through E82, suggesting that the amide hydrogens of these residues are solvent accessible and that they are not involved
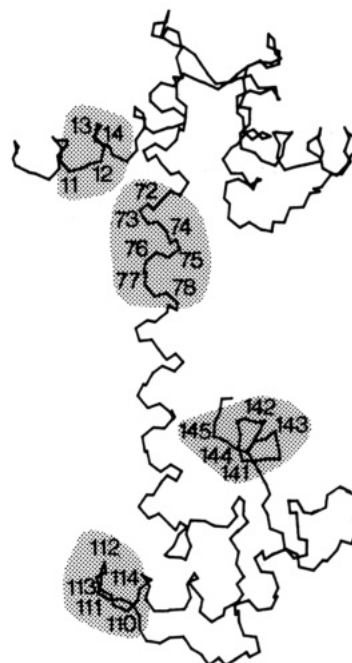

FIGURE 4: Crystal structure of calmodulin reported by Babu et al. (1988) with the four regions most affected by complexation with M13 shaded. Relatively large chemical shift changes are observed in the regions E11–E14, M72–D78, and F141–M145. A significant decrease in amide exchange rate is seen for residues T110–E114.

in strong hydrogen bonds. The absence of helical d_{NN} connectivity as well as the presence of "extended type" $d_{\alpha N}$ connectivity is also seen for residues K77 through E82 in M13-free CaM (Figure 3), and hydrogen-exchange experiments also show rapid exchange with solvent for these residues ($k_{exch} > 10$ s^{-1} at pH 7.0, 36 °C). Note that in the crystal structure this region is α-helical, albeit distorted (Kretsinger et al., 1986; Babu et al., 1988). NMR relaxation studies are presently in progress to measure the degree of flexibility for this structural element.

Seeholzer and Wand (1989) reported that for many of the amide protons a decrease in the exchange rate with solvent occurs upon complexation of CaM with target peptide. Most of the protons observed in their study are located in the interior of the two globular CaM domains and also exchange relatively slowly ($k_{exch} < 0.01$ s^{-1}) in the absence of target peptide. Our study of amide exchange rates focuses on relatively labile protons, mainly located on the surface of the protein. Upon complexation with M13, some of these protons actually increase their exchange rate with solvent (e.g., K75, K77, and K148). However, a significant decrease in the amide exchange rate was observed for residues T110, E112, G113, and E114 located at the end of the F helix of domain III. Downfield chemical shift changes for Cα and C' and upfield changes in Hα chemical shift observed in this region of the protein suggest a stabilization of the C-terminal end of the F helix of calcium-binding loop III, which these residues are part of. This is confirmed by medium-intensity d_{NN} NOE connectivities for residues R106–G113.

Figure 4 shows the crystal structure of CaM (Bahu et al., 1988), in which the three regions with the largest chemical shift changes and the hydrogen exchange protected C-terminal region of the F helix of domain III are shaded. This picture qualitatively supports the CaM–M13 model proposed by Persechini and Kretsinger (1988) where these shaded residues come into close proximity with the M13 peptide. In this model, the central helix is bent to bring the hydrophobic patches on the N- and C-terminal halves of the protein together, in such

Table I: Polypeptide Backbone ¹H, ¹³C, and ¹⁵N Chemical Shifts for *Drosophila* Calmodulin Complexed with M13 and Ca²⁺ and pH 6.8 and 36 °C and 0.1 M KCl[a]

	¹⁵N	Cα	C'	NH	Hα
A1		51.6	173.7		4.11
D2	120.5	54.5	175.6		4.68
Q3	120.0	55.4	175.7	8.37	4.41
L4	123.5	54.3	177.8	8.23	4.72
T5	113.1	60.3	175.3	8.75	4.53
E6	120.3	59.8	179.6	8.99	4.03
E7	119.7	59.6	178.5	8.23	4.15
Q8	118.7	58.5	179.6	7.74	4.09
I9	119.8	66.0	177.7	8.52	3.92
A10	121.7	55.2	180.8	8.05	4.16
E11	118.3	59.6	179.4	7.90	4.01
F12	117.0	62.5	178.9	8.30	4.66
K13	122.6	59.5	179.6	9.20	3.83
E14	119.8	59.3	180.1	8.52	4.12
A15	123.0	55.3	179.3	8.20	4.20
F16	118.9	61.6	178.1	8.88	3.45
S17	114.2	61.4	174.4	8.04	4.20
L18	119.8	56.6	177.6	7.48	4.12
F19	114.7	58.8	176.1	7.29	4.20
D20	116.6	51.7	176.8	7.66	4.55
K21	123.0	57.7	178.4	7.57	4.01
D22	114.0	52.5	177.8	8.12	4.62
G23	109.4	46.9	175.4	7.71	3.94/3.81
D24	121.2	53.3	177.4	8.52	4.55
G25	112.9	44.9	173.8	10.63	4.43/3.76
T26	111.7	59.1	173.3	8.21	5.47
I27	126.6	60.7	176.3	10.00	4.79
T28	116.3	59.0	176.7	8.46	4.89
T29	112.5	66.0	177.1	9.11	3.73
K30	120.6	58.8	179.9	7.57	4.13
E31	121.9	59.1	178.8	7.67	4.00
L32	120.4	57.8	179.0	8.72	4.08
G33	105.7	48.2	175.0	8.73	3.94/3.50
T34	117.9	66.7	177.1	7.90	3.97
V35	122.5	66.5	178.0	7.62	3.59
M36	116.6	58.2	179.2	8.52	4.10
R37	118.4	58.6	181.5	8.60	4.83
S38	119.4	61.6	175.0	8.05	4.32
L39	118.8	53.9	177.6	7.37	4.39
G40	107.1	45.3	174.6	7.85	4.32/3.84
Q41	118.5	53.9	174.3	7.99	4.50
N42	116.2	51.2	172.0	8.69	5.21
P43	136.4	62.1	177.7		4.85
T44	113.1	60.2	175.3	8.86	4.47
E45	120.3	59.7	178.9	8.79	4.01
A46	120.9	54.7	180.3	8.23	4.13
E47	118.6	58.8	179.8	7.68	4.10
L48	119.7	57.5	178.7	8.22	4.24
Q49	117.8	58.2	178.3	8.06	3.85
D50	120.3	57.3	178.9	7.97	4.49
M51	119.3	59.7	177.4	8.09	4.05
I52	116.1	63.4	178.2	7.55	3.62
N53	117.0	55.7	177.6	8.72	4.43
E54	116.1	57.9	177.2	7.58	4.15
V55	112.3	61.1	175.6	7.15	4.22
D56	121.5	53.3	176.1	7.86	4.53
A57	131.1	54.0	178.9	8.09	4.26
D58	114.0	52.4	178.0	8.26	4.67
G59	108.4	47.0	175.3	7.61	3.98/3.83
D60	118.9	52.3	176.9	8.21	4.65
G61	113.3	45.1	173.3	10.60	4.31/3.54
T62	108.1	59.0	173.4	7.65	4.80
I63	123.7	58.7	175.7	8.76	5.28
D64	128.9	51.8	176.1	9.12	5.51
F65	118.3	62.7	173.8	8.93	3.88
P66	137.6	66.6	179.8		3.85
E67	118.1	58.7	179.1	8.32	3.95
F68	124.1	61.0	176.2	8.59	3.93
L69	119.8	57.3	179.0	8.75	3.22
T70	115.0	66.3	176.4	7.93	3.66
M71	120.4	58.7	178.0	7.43	3.79
M72	114.7	54.0	177.1	7.51	4.36
A73	121.4	51.9	178.1	7.93	4.30
R74	118.6	56.3	176.2	7.06	4.15
K75	124.1	55.8	176.7	8.50	4.36
M76	123.8	54.6	176.2	8.64	4.54
K77	122.0	57.3	177.1	8.64	4.23
D78	120.2	55.5	176.4	8.59	4.54
T79	112.7	62.5	174.4	7.77	4.41
D80	123.9	54.2	177.4	8.21	4.76
S81	117.3	61.2	176.3	8.55	4.35
E82	121.6	59.2	178.6	8.37	4.14
E83	118.0	59.0	178.2	8.10	4.23
E84	119.8	58.9	179.9	7.99	4.12
I85	121.7	66.1	178.3	8.16	4.22
R86	122.6	60.0	179.2	8.44	4.19
E87	118.2	58.9	179.7	8.64	4.10
A88	121.2	55.3	179.2	8.07	4.23
F89	120.2	62.2	176.8	8.95	3.38
R90	115.2	58.4	177.1	7.99	3.97
V91	117.7	65.3	177.0	7.32	3.63
F92	114.9	60.6	176.5	7.12	4.20
D93	115.9	51.5	177.1	8.01	4.61
K94	125.1	58.9	178.4	7.48	3.94
D95	114.1	52.8	177.8	8.38	4.58
G96	109.4	46.9	175.2	7.88	3.91/3.91
N97	119.8	52.3	176.0	8.43	4.67
G98	112.6	44.5	172.7	10.71	4.09/3.46
F99	116.2	55.5	174.9	7.74	5.17
I100	127.3	61.0	175.7	10.28	4.75
S101	123.9	55.4	175.5	9.02	5.00
A102	123.1	55.6	179.2	9.32	3.95
A103	118.2	54.8	181.5	8.28	4.08
E104	120.3	59.0	179.6	7.92	4.05
L105	121.1	57.9	178.2	8.56	4.20
R106	117.2	59.7	178.7	8.71	3.76
H107	120.4	59.9	177.2	8.12	4.28
V108	118.4	66.4	178.0	7.98	3.57
M109	115.9	59.2	179.2	8.17	4.04
T110	114.7	66.1	178.5	8.44	4.12
N111	123.5	55.6	176.9	7.96	4.39
L112	118.6	55.7	176.7	7.78	4.10
G113	103.7	44.6	175.1	7.52	4.33/3.65
E114	121.5	55.6	175.4	8.08	4.41
K115	124.7	55.1	175.4	8.47	4.43
L116	125.2	53.8	177.2	8.12	4.86
T117	112.8	60.1	175.5	8.71	4.53
D118	121.1	57.8	178.7	8.87	4.27
E119	119.3	59.6	179.1	8.74	4.13
E120	120.2	58.8	179.7	7.67	4.01
V121	120.9	66.6	177.5	7.86	3.47
D122	119.8	57.4	179.1	8.02	4.38
E123	119.2	59.0	178.8	8.07	4.01
M124	119.4	59.6	180.2	7.71	4.32
I125	120.7	63.1	177.6	8.18	3.89
R126	117.9	59.5	179.1	8.42	4.11
E127	116.8	58.5	177.1	8.04	4.04
A128	117.4	51.1	177.5	7.20	4.38
D129	118.2	54.2	175.7	7.98	4.53
I130	128.1	63.4	177.9	8.27	3.91
D131	116.7	53.6	178.4	8.41	4.53
G132	108.6	47.0	175.4	7.65	4.01/3.84
D133	120.9	53.3	177.8	8.40	4.49
G134	112.6	45.4	172.8	10.29	4.09/3.46
Q135	115.0	53.0	175.1	8.00	4.97
V136	125.4	61.4	176.0	9.16	5.24
N137	129.4	50.6	174.8	9.66	5.38
Y138	118.4	62.0	176.3	8.29	3.29
E139	118.9	59.8	180.5	8.07	3.64
E140	120.9	58.5	179.2	8.88	3.83
F141	123.8	61.4	176.4	8.46	3.53
V142	119.4	66.7	179.4	8.78	3.03
T143	118.3	66.7	175.9	8.03	3.65
M144	119.3	56.9	177.5	7.38	4.15
M145	112.8	55.1	177.4	7.50	3.91
T146	107.9	61.3	174.7	7.55	4.39
S147	118.4	58.4	173.7	7.56	4.47
K148	128.5	57.6	181.5	8.09	4.15

[a] ¹H chemical shifts are expressed relative to (trimethylsilyl)propionic-d_4 acid (TSP), ¹³C chemical shifts are relative to hypothetically internal TSP, where 0 ppm is obtained by multiplying the ¹H TSP frequency by 0.25144954. ¹⁵N shifts are relative to external liquid ammonia at 25 °C, where 0 ppm has been obtained by multiplying the 0 ppm ¹H TSP frequency by 0.10132914.

a way that both can interact simultaneously with M13. A fundamentally similar model for calmodulin when binding to a number amphiphilic helical peptides was supported by extensive photoaffinity labeling and fluorescence results (O'Neill & DeGrado, 1989, 1990). In the Kretsinger and Persechini model, only a single dihedral backbone angle, the ψ angle of S81, needed to be changed significantly from the crystallographic structure to accommodate M13 binding. The NOE data summarized in Figure 3 indicate that a more substantial backbone rearrangement takes place, involving residues 75 through 81.

A more detailed structural analysis of the CaM–M13 complex requires complete side-chain assignments not only for CaM but also for M13, followed by a time-consuming analysis of the NOE data. This work is presently in progress, and we are optimistic about the possibility of obtaining a high-resolution solution structure for the CaM–M13 complex.

SUPPLEMENTARY MATERIAL AVAILABLE

Two figures (3 pages) showing ¹⁵N–¹H shift correlation spectra of CaM and the CaM–M13 complex, cross sections

of 3D HCACO, 3D HCA(CO)N, and 4D HCACON for D24 and D56. Ordering information is given on any current masthead page.

Registry No. MLCK, 51845-53-5.

REFERENCES

Anderson, S. R., & Malencik, D. A. (1986) in *Calcium Cell Function* (Cheung, W. Y., Ed.) Vol. 6, pp 1–42, Academic Press, New York.

Babu, Y. S., Bugg, C. E., & Cook, W. J. (1988) *J. Mol. Biol. 204*, 191–204.

Bax, A., Clore, G. M., & Gronenborn, A. M. (1990) *J. Magn. Reson, 88*, 425–431.

Blumenthal, D. K., & Krebs, E. G. (1988) in *Molecular Aspects of Cellular Regulation* (Cohen, P., & Klee, C. B., Eds.) Vol. 5, pp 341–356, Elsevier, New York.

Blumenthal, D. K., Takio, K., Edelman, A. M., Charbonneau, H., Titani, K., Walsh, K. A., & Krebs, E. G. (1985) *Proc. Natl. Acad. Sci. U.S.A. 82*, 3187–3191.

Bodenhausen, G., & Ruben, D. J. (1980) *Chem. Phys. Lett. 69*, 185–189.

Clayden, N. G., & Williams, R. J. P. (1982) *J. Magn. Reson. 49*, 383–396.

Clore, G. M., Bax, A., Driscoll, P. C., Wingfield, P. T., Gronenborn, A. M. (1990) *Biochemistry 29*, 8172–8184.

Fesik, S. W., Eaton, H. L., Olejniczak, E. T., Zuiderweg, E. R. P., McIntosh, L. P., & Dahlquist, F. W. (1990) *J. Am. Chem. Soc. 112*, 886–887.

Glushka, J., Lee, M., Coffin, S., & Cowburn, D. (1989) *J. Am. Chem. Soc. 111*, 7716–7722.

Heidorn, D. B., Seeger, P. A., Rokop, S. E., Blumenthal, D. K., Means, A. R., Crespi, H., & Trewhella, J. (1989) *Biochemistry 28*, 6757–6764.

Ikura, M., Hasegawa, N., Aimoto, S., Yazawa, M., Yagi, K., & Hikichi, K. (1989) *Biochem. Biophys. Res. Commun. 161*, 1233–1238.

Ikura, M., Kay, L. E., & Bax, A. (1990a) *Biochemistry 29*, 4659–4667.

Ikura, M., Marion, D., Kay, L. E., Shih, H., Krinks, M., Klee, C. B., & Bax, A. (1990b) *Biochem. Pharmacol. 40*, 153–160.

Jackson, A. E., Carraway, K. L., Puett, D., & Brew (1986) *J. Biol. Chem. 261*, 12226–12232.

Kataoka, M., Head, J. F., Seaton, B. A., & Engelman, D. M. (1989) *Proc. Natl. Acad. Sci. U.S.A. 86*, 6944–6948.

Kay, L. E., Marion, D., & Bax, A. (1989) *J. Magn. Reson. 84*, 72–84.

Kay, L. E., Ikura, M., & Bax, A. (1990a) *J. Am. Chem. Soc. 112*, 888–889.

Kay, L. E., Ikura, M., Tschudin, R., & Bax, A. (1990b) *J. Magn. Reson. 89*, 496–514.

Kay, L. E., Ikura, M., & Bax, A. (1991a) *J. Magn. Reson. 91*, 84–92.

Kay, L. E., Ikura, M., Zhu, G., & Bax, A. (1991b) *J. Magn. Reson. 91*, 422–428.

Klee, C. B. (1988) in *Molecular Aspects of Cellular Regulation* (Cohen, P., & Klee, C. B., Eds.) Vol. 5, pp 35–56, Elsevier, New York.

Klevit, R. E., Blumenthal, D. K., Wemmer, D. E., & Krebs, G. E. (1985) *Biochemistry 24*, 8152–8157.

Kretsinger, R. H., Rudnick, S. E., & Weissman, L. J. (1986) *J. Inorg. Biochem. 28*, 289–302.

Linse, S., Drakenberg, T., & Forsen, S. (1988) *FEBS Lett. 119*, 28–32.

Manalan, A. S., & Klee, C. B. (1987) *Biochemistry 26*, 1382–1390.

Marion, D., Ikura, M., Tschudin, R., & Bax, A. (1989a) *J. Magn. Reson. 85*, 393–399.

Marion, D., Driscoll, P. C., Kay, L. E., Wingfield, P. T., Bax, A., Gronenborn, A. M., & Clore, G. M. (1989b) *Biochemistry 28*, 6150–6156.

Matsushima, N., Izumi, Y., Matsuo, T., Yoshino, H., Ueki, T., & Miyake, Y. (1989) *J. Biochem. (Tokyo) 105*, 883–887.

Messerle, B. A., Wider, G., Otting, G., Weber, C., & Wuthrich, K. (1989) *J. Magn. Reson. 85*, 608–613.

O'Neil, K. T., & Degrado, W. F. (1989) *Proteins 6*, 284–293.

O'Neil, K. T., & Degrado, W. F. (1990) *Trends Biochem. Sci. 15*, 50–64.

Pastore, A., & Saudek, V. (1990) *J. Magn. Reson. 90*, 165–176.

Persechini, A., & Kretsinger, R. H. (1988) *J. Cardiovas. Pharmacol. (S5) 12*, 1–12.

Roy, S., Papastavros, Z., Sanchez, W., & Redfield, A. G. (1984) *Biochemistry 23*, 4395–4400.

Saito, H. (1986) *Magn. Reson. Chem. 24*, 835–852.

Seeholzer, S. H., & Wand, A. J. (1989) *Biochemistry 28*, 4011–4020.

Seeholzer, S. H., Cohen, M., Putkey, J. A., Means, A. R., & Crespi, H. I. (1986) *Proc. Natl. Acad. Sci. U.S.A. 83*, 3634–3638.

Shoji, A., Ozaki, T., Fujito, T., Deguchi, K., & Ando, I. (1987) *Macromolecules 20*, 2441–2445.

Spera, S., Ikura, M., & Bax, A. (1991) *J. Biomol. Nucl. Magn. Reson.* (in press).

Szilagyi, L., & Jardetzky, O. (1989) *J. Magn. Reson. 83*, 441–449.

Wagner, G., Pardi, A., & Wuthrich, K. (1983) *J. Am. Chem. Soc. 105*, 5948–5949.